BJP BRITISH JOURNAL OF PHARMACOLOGY

BPS BRITISH PHARMACOLOGICAL SOCIETY

British Journal of Pharmacology (2010), 159, 405–418

0007-1188/09
www.brjpharmacol.org

RESEARCH PAPER

Mechanisms of $K_v2.1$ channel inhibition by celecoxib – modification of gating and channel block

RV Frolov[1,2], VE Bondarenko[3,4] and S Singh[1]

[1]*Department of Pharmacology and Toxicology, State University of New York, Buffalo, New York, USA,* [2]*Department of Physical Sciences, Division of Biophysics, University of Oulu, Oulun Yliopisto, Finland,* [3]*Department of Physiology and Biophysics, State University of New York, Buffalo, New York, USA, and* [4]*Department of Mathematics and Statistics, Georgia State University, Atlanta, GA, USA*

Background and purpose: Selective cyclooxygenase-2 (COX-2) inhibitors such as rofecoxib (Vioxx) and celecoxib (Celebrex) were developed as NSAIDs with reduced gastric side effects. Celecoxib has now been shown to affect cellular physiology via an unexpected, COX-independent, pathway – by inhibiting $K_v2.1$ and other ion channels. In this study, we investigated the mechanism of the action of celecoxib on $K_v2.1$ channels.
Experimental approach: The mode of action of celecoxib on rat $K_v2.1$ channels was studied by whole-cell patch-clamping to record currents from channels expressed in HEK-293 cells.
Key results: Celecoxib reduced current through $K_v2.1$ channels when applied from the extracellular side. At low concentrations ($\leq$3 μM), celecoxib accelerated kinetics of activation, deactivation and inactivation. Recovery of rat $K_v2.1$ channels from inactivation could be characterized by two components, with celecoxib selectively accelerating the slow component of recovery at $\leq$10 μM. At >3 μM, celecoxib led to closed-channel block with relative slowing of activation. At 30 μM, it additionally induced open-channel block that manifested in use-dependent inhibition and slower recovery from inactivation.
Conclusions and implications: Celecoxib reduced current through $K_v2.1$ channels by modifying gating and inducing closed- and open-channel block, with the three effects manifesting at different concentrations. These data will help to elucidate the mechanisms of action of this widely prescribed drug on ion channels and those underlying its neurological, cardiovascular and other effects.
British Journal of Pharmacology (2010) **159,** 405–418; doi:10.1111/j.1476-5381.2009.00539.x; published online 15 December 2009

Keywords: celecoxib; celebrex; $K_v2.1$ channels; gating modification; closed-channel block; open-channel block; selective cyclooxygenase-2 inhibitor; NSAID

Abbreviations: 4-AP, 4-amino pyridine; COX, cyclooxygenase; EC, equivalent charge; HP, holding potential; LC, liquid chromatography; NMR, nuclear magnetic resonance; τ_{act}, time constant for activation; τ_{deact}, time constant for deactivation; τ_{inact}, time constant for inactivation; $V^a_{1/2}$, half activation potential; $V^i_{1/2}$, half inactivation potential

Introduction

The importance of selective inhibitors of cyclooxygenase-2 (COX-2) stems from their use as non-steroidal anti-inflammatory drugs (NSAIDs) with relatively less gastric side-effects (Flower, 2003). Non-selective NSAIDs irreversibly inhibit both isoforms of cyclooxygenase, a house-keeping COX-1 and an inducible COX-2 (Kalgutkar *et al.*, 1998). Gastrointestinal side effects of NSAIDs are associated with inhibition of gastric COX-1 that mediates the synthesis of the gastroprotective prostaglandin E_2 (Singh and Triadafilopoulos, 1999). Indeed, the main concept underlying the development of selective COX-2 inhibitors, or coxibs, was to create a 'safer aspirin' (Burnier, 2005). After being introduced to the market, coxibs (rofecoxib, valdecoxib and celecoxib) quickly became the NSAIDs of choice. After the withdrawal of rofecoxib (Vioxx) in 2004 and of valdecoxib (Bextra) in 2005 due to their cardiovascular and other side effects, celecoxib (Celebrex, Pfizer, New York, NY, USA) remains the only approved coxib in the United States, with more than one million prescriptions per month (Brownstein *et al.*, 2007).

Several studies show that celecoxib can target enzymatic and cellular mechanisms other than cyclooxygenases. It inhibits carbonic anhydrases with nanomolar affinity (Weber

Correspondence: Dr Satpal Singh, Department of Pharmacology and Toxicology, 102 Farber Hall, State University of New York at Buffalo, Buffalo, NY 14214-3000, USA. E-mail: singhs@buffalo.edu
Received 27 November 2008; revised 30 August 2009; accepted 10 September 2009

et al., 2004). It also inhibits voltage-gated Na^+ channels in rat dorsal root ganglion neurones and Ca^{2+} channels in rat pheochromocytoma (PC12) cells (Park *et al*., 2007; Zhang *et al*., 2007). In addition, it inhibits voltage-gated K^+ and Na^+ channels and leads to a striking suppression of spontaneous spike activity in rat isolated retinal neurones (Frolov *et al*., 2008a).

We have previously reported (Frolov *et al*., 2008b) that celecoxib can reduce heart rate and induce dysrhythmia in *Drosophila*. These effects occur in spite of the genomic absence of cyclooxygenases in *Drosophila* and are mediated by the inhibition of Shab (K_v2) K^+ channels (Hegde *et al*., 1999; Singh and Singh, 1999; Chopra *et al*., 2000). Celecoxib similarly lowers the rate of beating of rat ventricular myocytes in culture and significantly increases irregularity of beating by inhibiting $K_v2.1$ channels (Frolov *et al*., 2008b).

$K_v2.1$ channels (nomenclature follows Alexander *et al*., 2008) are widely expressed in various tissues in mammals, including humans. They are found in cardiomyocytes (Ordog *et al*., 2006), skeletal muscles (Wang *et al*., 2002), vascular smooth muscles (Patel *et al*., 1997), placental vasculature (Wareing *et al*., 2006), pancreatic β-cells (Yan *et al*., 2004) and retina (Pinto and Klumpp, 1998). They are expressed at very high levels in virtually all brain neurones (Baranauskas *et al*., 1999; Murakoshi and Trimmer, 1999; Misonou *et al*., 2005). In mammalian central nervous system neurones, $K_v2.1$ channels conduct a predominant, delayed rectifier, K^+ current that regulates neuronal excitability, action potential duration and tonic spiking (Malin and Nerbonne, 2002; Misonou *et al*., 2004).

Because of the wide use of celecoxib and the significant role played by $K_v2.1$ channels in a number of physiological processes, it is important to understand the mechanisms underlying the inhibition of these channels by the drug. Reduction in whole-cell current in the presence of an exogenous compound may result from a channel block, a change in channel kinetics and/or a change in the number of functional channels. In this study, we examined if celecoxib blocked the channels and/or if it altered their kinetic properties. For this purpose, we analysed the effect of celecoxib on rat $K_v2.1$ ($rK_v2.1$) channels expressed in HEK-293 cells. Our data show the contribution of gating modifications and of closed- as well as open-channel block to the overall effects of celecoxib on $K_v2.1$ channels.

Methods

Expression of rat $K_v2.1$ channels in HEK-293 cells

The pcDNA-$K_v2.1$ vector was provided by Dr. H. Y. Gaisano at the University of Toronto (Leung *et al*., 2003). HEK-293 cells were grown in DMEM (Dulbecco's Modified Essential Medium) supplemented with 100 units·mL^{-1} penicillin and 100 μg·mL^{-1} streptomycin (Invitrogen Corporation, CA, USA) at 37°C in 5% CO_2. One day before transfection, cells were plated on 35 mm Falcon culture dishes (Becton Dickinson Labware, Franklin Lakes, NJ, USA). On the next day, 6 μL of FuGene 6 transfection reagent (Roche Molecular Biochemicals, IN, USA), 2 μL of solution containing 1.5 μg pcDNA-$K_v2.1$ and 2 μL of solution containing 0.2 μg pEGFP-N2 were added to an Eppendorf tube with 190 μL of DMEM and gently shaken. After 30 min of incubation at room temperature, the contents of the tube were added to the dish with HEK-293 cells. Recordings were performed 24–48 h after transfection.

Electrophysiology and data analysis

Whole-cell current recordings from HEK-293 cells expressing rat $K_v2.1$ channels and data analysis were performed by using an Axopatch 200B amplifier and pClamp 9.2 software (Axon Instruments/Molecular Devices, CA, USA). Patch electrodes were fabricated from thin-walled borosilicate glass (World Precision Instruments, Sarasota, FL, USA). Electrodes had a resistance of 2.3–3.5 MΩ. Patch pipettes contained (in mM) 140 KCl, 5.4 NaCl, 2 $MgCl_2$, 1 $CaCl_2$, 11 EGTA and 10 HEPES (pH 7.2). Bath solution contained (in mM) 140 NaCl, 4.7 KCl, 1.2 $MgCl_2$, 2.5 $CaCl_2$, 10 HEPES and 11 glucose (pH 7.4).

Series resistance or capacitance compensation was not performed because the HEK-293 cells were very sensitive to high levels of correction. In practice, however, capacitance compensation was not needed because the membrane time constant, measured from the capacitive transient, varied from a few hundred μs to less than 1 ms, while the time to peak even at the highest used voltage of +40 mV showed a range of 10–20 ms. Similarly, access resistance was low, and, during data analysis, we used cells with access resistance of less than 10 MΩ. As a result, the time constant for activation (τ_{act}) was not significantly affected over a peak-current range of 2–8 nA observed in response to a pulse to +40 mV.

Experiments were performed either under conditions of continuous exposure of HEK-293 cells to various concentrations of celecoxib in bath solution or using a custom-made perfusion system, as indicated in the figure legends. The experiments were performed at 21–23°C.

Experimental protocols

Repetitive stimulation of a cell resulted in significant long-term facilitation of $K_v2.1$ current at negative voltages (between –30 and 0 mV), with a hyperpolarizing shift of the half-activation potential. Similar observations have been reported previously for $K_v2.1$ channels and linked to dephosphorylation and declustering of normally heavily phosphorylated (Park *et al*., 2006) and densely packed $K_v2.1$ channels in neurones or $K_v2.1$ channels exogenously expressed in mammalian cell lines (Mohapatra *et al*., 2007). Such facilitation complicates the interpretation of data obtained by recording from the same cell subjected to multiple runs of an experimental protocol (e.g. to measure cellular response to the drug, we have to run the experimental protocol twice, before and after the application of the drug). For this complication to be avoided, the currents were recorded from different cells with a single run of experimental protocol in control or in the presence of celecoxib. For the error resulting from comparison of currents produced by different cells to be decreased, the following experimental strategies were utilized. First, only HEK-293 cells displaying moderate green fluorescence were used in experiments, resulting in $K_v2.1$ current amplitude of 3.0 ± 0.2 nA in control at +40 mV (n = 40). Second, cells from the same dish were used to study effects of

different concentrations of celecoxib, ensuring lower variability in current amplitudes, caused by differences in cell conditions and transfection success. In addition, a relatively large number of cells were used in analysis of celecoxib's effects on $K_v2.1$ amplitude ($n > 10$). In the figures showing normalized currents, normalization was performed by using the average current amplitudes in control unless stated otherwise.

Computer simulations

To investigate if the observed effects on activation and inactivation kinetics could reduce $K_v2.1$ currents to the extent observed in our experiments, we generated model current traces using averaged experimental data on time constants of activation and inactivation. The current traces were simulated by the function

$$f_t(t) = I_{ampl}[1 - \exp(-t/\tau_{act})]^4 \times [C_1\exp(-t/\tau_{inact1}) + C_2\exp(-t/\tau_{inact2}) + C_3], \quad (1)$$

where I_{ampl} is the experimental average peak current amplitude in control, τ_{act} and $\tau_{inact1,2}$ are the average experimental activation and inactivation time constants, respectively, and C_1, C_2 and C_3 are the constants obtained by fitting current decay (inactivation) with bi-exponential function, such that $C_1 + C_2 + C_3 = 1$. To simulate the effects of gating modification, we used the values of τ_{act}, $\tau_{inact1,2}$ and constants C_1, C_2 and C_3 from the control sample and in the presence of celecoxib, while the value of I_{ampl} was the same as in the control sample. Comparison of these simulations with corresponding experimental data allowed finding the differences in peak currents that could not be attributed to gating modification alone.

Curve fitting

$K_v2.1$ channels are formed by tetramers with four identical subunits (Birnbaum *et al.*, 2004). While individual subunits can be considered as being activated independently, the channel pore becomes permeable to ions when all four subunits have been activated. Thus, a fourth-order Boltzmann function $f_a(V) = 1/(1 + \exp(-(V - V^a_{1/2})/b))^4$, where $V^a_{1/2}$ is the half-activation potential and b is the slope factor, was used to fit voltage dependence of fractional maximal conductance g/g_{max} (Wang *et al.*, 2004). Similarly, fitting of activation time courses can be explained by fourfold symmetry of $K_v2.1$. Thus, the function $f_a(t) = C(1 - \exp(-t/\tau_{act}))^4$ was used to fit rising parts of the current traces to obtain the values of the activation time constant, τ_{act} (Wang *et al.*, 2004).

Inactivation time courses of the currents in control, without exposure to celecoxib, was well fitted by a mono-exponential function. Bi-exponential function provided only a marginal improvement to the fit of the control traces. However, a bi-exponential function was needed to fit inactivation data at >0.3 μM celecoxib, as it provided a much better fit to the experimental data than the mono-exponential function. Similarly, a bi-exponential function produced a better fit than a mono-exponential function for recovery from inactivation.

Statistical analysis

Data were compared by single factor ANOVA or paired, two sample for means *t*-test, where indicated. All values are means ± SEM; (*): $P < 0.05$, (**): $P < 0.01$ (ANOVA).

Materials. Fifteen 200-mg capsules of Celebrex, obtained from a local pharmacy, were disassembled, and the contents were suspended in 50 mL of high performance liquid chromatography (HPLC)-grade methanol. The mixture was stirred for 15 h and filtered through a small pad of Celite, and the filter cake was washed with 5 mL of methanol. The combined filtrates were concentrated and the residue was recrystallized from acetonitrile. The white powder was collected by filtration to give 1.50 g (50%) of celecoxib (4-[5-(4-methylphenyl)-3-(trifluoromethyl)-1H-pyrazol-1-yl]benzenesulphonamide) as a white powder, which was characterized by LC mass spectrometry with electrospray ionization (*m/z* 380 for $M + H^+$) and by ^1H nuclear magnetic resonance (NMR) spectroscopy [(CD_2Cl_2) δ 7.89 (AA'BB', 2 H, *J* = 2, 7 Hz), 7.48 (AA'BB', 2 H, *J* = 2, 7 Hz), 7.19 (AA'BB', 2 H, *J* = 2, 6 Hz), 7.13 (AA'BB', 2 H, *J* = 2, 6 Hz), 6.77 (s, 1 H), 4.96 (br s, 2 H), 2.37 (s, 3 H)]. LC mass spectrometry and NMR spectroscopy did not show the presence of any significant detectable impurities (>98% purity). We have also used the capsule contents without extraction, as described above, in experiments, and no difference between the effects of the extracted and unextracted compound was detected. Most other chemicals used in preparing solutions were obtained from Sigma-Aldrich (St. Louis, MO, USA).

Results

Dose–response relationships

As reported previously (Frolov *et al.*, 2008a,b), extracellular application of celecoxib accelerated inactivation of $rK_v2.1$ channels expressed in HEK-293 cells (Figure 1A, inset). Dose–response correlations for the peak current and for the current at the end of a 4 s voltage pulse, when the fast inactivation processes had set in (Figure 1A), provided IC_{50} values of 9.1 μM and 2.6 μM, respectively.

Activation

The current showed a threshold for activation of about –40 mV, and the peak current-voltage relationships were linear at voltages positive to –10 mV (Figure 1A). To investigate the voltage dependence of current inhibition, we plotted ratios of averaged peak currents in the presence of 3, 10 and 30 μM celecoxib to those in control as a function of voltage (Figure 1B). Figure 1B shows that $rK_v2.1$ current reduction was larger at the negative than the positive voltages, suggesting a mechanism that is different from open-channel block.

Rat $K_v2.1$ channels typically respond to depolarization by relatively slow activation. Activation time course demonstrated a sigmoid delay with or without celecoxib (Figure 2A, B). Figure 2C shows the voltage dependence of τ_{act} in control and with different concentrations of celecoxib. The drug significantly decreased τ_{act} between –20 and +10 mV, with a smaller effect at higher potentials (Figure 2, A–C). At –20 mV,

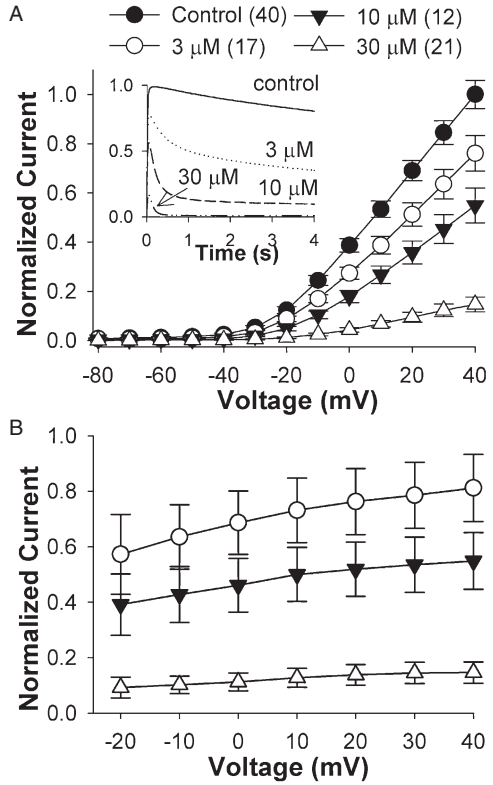

Figure 1 Inhibition of $rK_v2.1$ channels by celecoxib. (A) Peak current-voltage relationships (I–V) are shown in control conditions and during exposure to different concentrations of celecoxib. The inset shows reduction in current amplitude and acceleration of inactivation by extracellularly applied celecoxib. It shows averaged currents from HEK-293 cells expressing $rK_v2.1$ channels in control and at different concentrations of celecoxib during a 4000-ms depolarizing pulse from a holding potential (HP) of –80 mV to +40 mV. (B) Voltage dependence of peak current inhibition is shown at various concentrations. The value plotted at each point was obtained as the ratio between the normalized current for a given celecoxib concentration (as shown in panel A) to the corresponding control value shown in panel A (see Methods). Symbols are the same as in panel A. *n*, number of experiments.

the values of τ_{act} were 27.5 ± 2.0 ms (control), 16.9 ± 1.7 ms (3 μM, $P < 0.0001$) and 16.6 ± 1.2 ms (10 μM, $P < 0.001$). At 0 mV, they were 10.8 ± 0.8 ms (control), 7.4 ± 0.6 ms (3 μM, $P < 0.01$) and 7.9 ± 0.5 ms (10 μM, $P < 0.01$).

Importantly, the τ_{act} values at 10 μM were consistently larger than those at 3 μM. Due to small current amplitudes with 30 μM celecoxib, it was not possible to determine τ_{act} at –20 mV, but, at higher voltages, τ_{act} at 30 μM were larger than those obtained at 3 and 10 μM. For example, at +40 mV (Figure 2C, inset), the activation time constants decreased up to concentrations of 3 μM and increased at concentrations >3 μM, with the smallest value of 3.7 ± 0.3 ms at 3 μM and the largest value of 4.8 ± 0.3 ms ($P < 0.02$) at 30 μM celecoxib.

Equivalent charge (EC) of activation, a quantitative measure of the voltage dependence, was determined by fitting the voltage dependence of τ_{act} with a single exponential function, $\tau_{act} = \tau_{act0} \times \exp(-V/V_{act}) + \tau_{actC}$, where τ_{act0}, τ_{actC} and V_{act} are the fitting constants. The EC was calculated by using equation $z_a = -k_BT/e_0V_{act}$, where k_B is the Boltzmann constant, T is the absolute temperature and e_0 is the elementary charge. The EC was 4.05 ± 0.10 in control, 3.80 ± 0.15 at 3 μM, 3.58 ± 0.17 at 10 μM ($P < 0.01$) and 2.7 ± 0.27 at 30 μM ($P < 0.0001$) per channel subunit. Although these estimates of EC provide only a minimal value of the charge movement per subunit, a significant dose-dependent decrease of activation EC is consistent with acceleration of the activation kinetics of $rK_v2.1$ channels. Thus, the application of 10 and 30 μM celecoxib resulted in a less steep voltage-dependence of activation than in the control. The voltage-independent constant value τ_{actC} determines the rate-limiting step in activation pathway of $K_v2.1$ channels (Wang *et al.*, 2004). Our data indicate that τ_{actC} does not change at different concentration of celecoxib and was 3.61 ± 0.1 ms. At relatively large depolarizations (+30 to +50 mV), this rate is primarily responsible for activation time constant, and contribution of voltage-dependent steps, affected by celecoxib, in channel activation is relatively small. This results in a greater sensitivity of the τ_{act} of $K_v2.1$ channels to celecoxib at relatively small depolarizations, between –20 and +10 mV.

Values of half-activation potential, $V^a_{1/2}$, were determined from the voltage dependence of the fractional maximal conductance g/g_{max} (Figure 2D). Celecoxib did not affect the values of $V^a_{1/2}$, which were –31.8 ± 1.3 mV in control, –31.9 ± 1.7 mV at 0.3 μM, –29.2 ± 1.7 mV at 1 μM, –32.8 ± 1.7 mV at 3 μM, –30.1 ± 2.1 mV at 10 μM and –28.4 ± 1.7 mV at 30 μM.

Deactivation

Deactivation is the reverse process to activation. Deactivating tail current kinetics were voltage-dependent and significantly faster in the presence of celecoxib than in the control (Figure 3). Deactivation time constants (τ_{deact}) at –60 mV were 15.4 ± 0.6 ms in control, 11.3 ± 1.5 ms at 3 μM ($P < 0.05$), 7.9 ± 0.5 ms at 10 μM ($P < 0.001$) and 5.7 ± 0.2 ms at 30 μM ($P < 0.001$). Voltage dependence of τ_{deact} was not significantly affected by celecoxib, with the EC of deactivation being 3.50 ± 0.28 in control, 3.09 ± 0.55 at 3 μM, 3.46 ± 0.47 at 10 μM and 2.90 ± 0.73 at 30 μM.

A characteristic feature of open-channel block is the deceleration of deactivation in the presence of a blocker. For a blocked channel to close (deactivate), an open-channel blocker must first dissociate from the channel pore. As a typical rate of unbinding for the majority of blockers is much lower than the rate of open-to-close transition, this additional step often results in an increase of τ_{deact} and may manifest in the 'cross-over' of tail currents (Gonzalez *et al.*, 2002; Wang *et al.*, 2003). Although celecoxib reduced peak currents, its effect on deactivation was quite opposite to that of an open-channel blocker at drug concentrations less than 30 μM. It resulted in a substantial concentration-dependent acceleration of deactivation, and did not demonstrate 'cross-over' (Figure 3, A–C). At 30 μM, celecoxib further accelerated the deactivation of $K_v2.1$ channels at –60 and –50 mV, which is consistent with concentration-dependent acceleration of deactivation due to gating modification. Interestingly, τ_{deact} at 30 μM did not further decrease at more hyperpolarized potentials (between –70 and –110 mV).

Inactivation

The most apparent effect of celecoxib was a dramatic acceleration of normally slow inactivation of $rK_v2.1$ channels

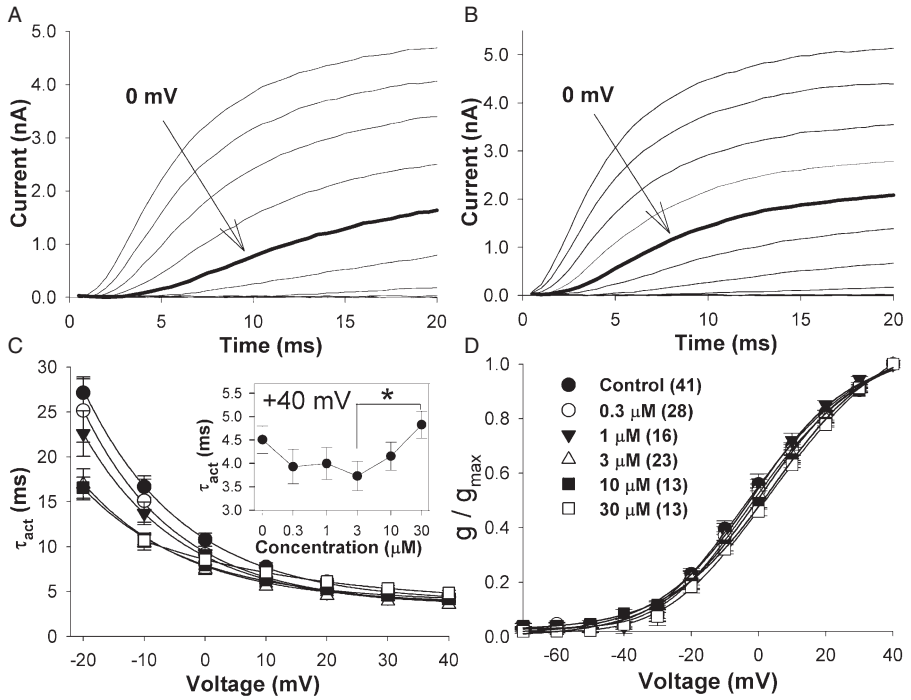

Figure 2 Effects of celecoxib on activation of $rK_v2.1$ channels. The rising current is characterized by a sigmoid time course in control conditions (A) and in the presence of celecoxib (B). Current traces were obtained during depolarizing pulses between −70 and +40 mV in 10 mV voltage steps (HP = −80 mV). The rising phase of the current, as measured between the beginning of the current trace and the current maximum, was accelerated by celecoxib, especially at negative potentials. (C) Voltage dependence of τ_{act} at different concentrations of celecoxib. Values of τ_{act} were determined by fitting the rising phase of $rK_v2.1$ channel current with a function $f_a(t) = C(1 - \exp(-t/\tau_{act}))^4$. Power index 4 reflects independent gating of each of the four $K_v2.1$ channel α-subunits during activation. Inset in panel C shows concentration dependence of τ_{act} at +40 mV. (D) voltage-dependence of the fractional maximum conductances g/g_{max} is shown under control conditions and during exposure to different concentrations of celecoxib. $V^a_{1/2}$ values were determined by fitting data with a fourth-power Boltzmann function, $f_a(V) = 1/(1 + \exp(-(V - V^a_{1/2})/b))^4$, where b is the slope factor; (*n*), number of experiments.

(Figure 4). Inactivation kinetics were examined during 4000-ms pulses. The time course of inactivation in control was described with a mono-exponential function. Even a 60-s voltage step to +40 mV did not elicit a second component of inactivation (data not shown).

The drug caused a large hyperpolarizing shift of half-inactivation potential ($V^i_{1/2}$). The values of $V^i_{1/2}$ were −17.6 ± 2.3 mV in control, −23.3 ± 2.9 mV at 0.3 μM, −28.8 ± 2.8 mV at 1 μM ($P < 0.01$), −33.6 ± 2.8 mV at 3 μM ($P < 0.001$), and −36.6 ± 2.1 mV at 10 μM ($P < 0.001$) (Figure 4C).

The effect of celecoxib on inactivation time constants (τ_{inact}) was concentration dependent (Figure 5). At 0.3 μM, values of τ_{inact} were reduced by ~30% (Figure 5). At higher concentrations, celecoxib introduced a new component of inactivation, and the best fit of inactivation time course was obtained with a bi-exponential function (Figure 5A). Fitting accuracy was estimated by the formula $\Delta = \frac{1}{N}\left[\sum_{i=1}^{N}\left(I^{exper}_{Kv2.1} - I^{fit}_{Kv2.1}\right)^2\right]^{1/2}$, where $I^{exper}_{Kv2.1}$ and $I^{fit}_{Kv2.1}$ refers to the experimental data and the fitting data (with mono-exponential and bi-exponential functions) and *N* is the number of experimental points. The values of Δ were equal to 1.35 and 0.23 pA for the fits with mono-exponential and bi-exponential functions, respectively.

The slow component of inactivation is shown in Figure 5B, and the fast component in Figure 5C. τ_{inact} decreased in dose-dependent manner with an increase of contribution of the fast component at higher concentrations: the fractional amplitude of the fast component increased from 17 ± 3% at 1 μM to 79 ± 3% at 10 μM celecoxib (Figure 5C).

We also examined the effect of 3 μM celecoxib on the kinetics of closed-state inactivation at −60 mV. The experimental protocol consisted of four pulses (HP = −80 mV): P1 (+40 mV, 100-ms duration), P2 (−80 mV, 5000-ms duration), P3 (−60 mV, variable duration ranging from 2000 to 17 200 ms) and P4 (+40 mV, 100-ms duration). Normalized peak current (P4/P1) representing the fraction of non-inactivated current after variable exposure to sub-threshold potential of −60 mV was used to assess the extent of closed-state inactivation. Very little closed-state inactivation was detected at −60 mV in control, with 3 μM celecoxib showing no effect (data not shown).

Recovery from inactivation

We next tested the effect of celecoxib on recovery of $rK_v2.1$ channel from inactivation. The time course of recovery in control and in the presence of celecoxib was bi-exponential (Figure 6). Fitting accuracy was estimated by the formula for Δ as given in the preceding section on Inactivation. The values of Δ were equal to 0.0034 and 0.0012 for the fits with mono-exponential and bi-exponential functions, respectively (threefold increase in fitting accuracy with bi-exponential function compared with mono-exponential function).

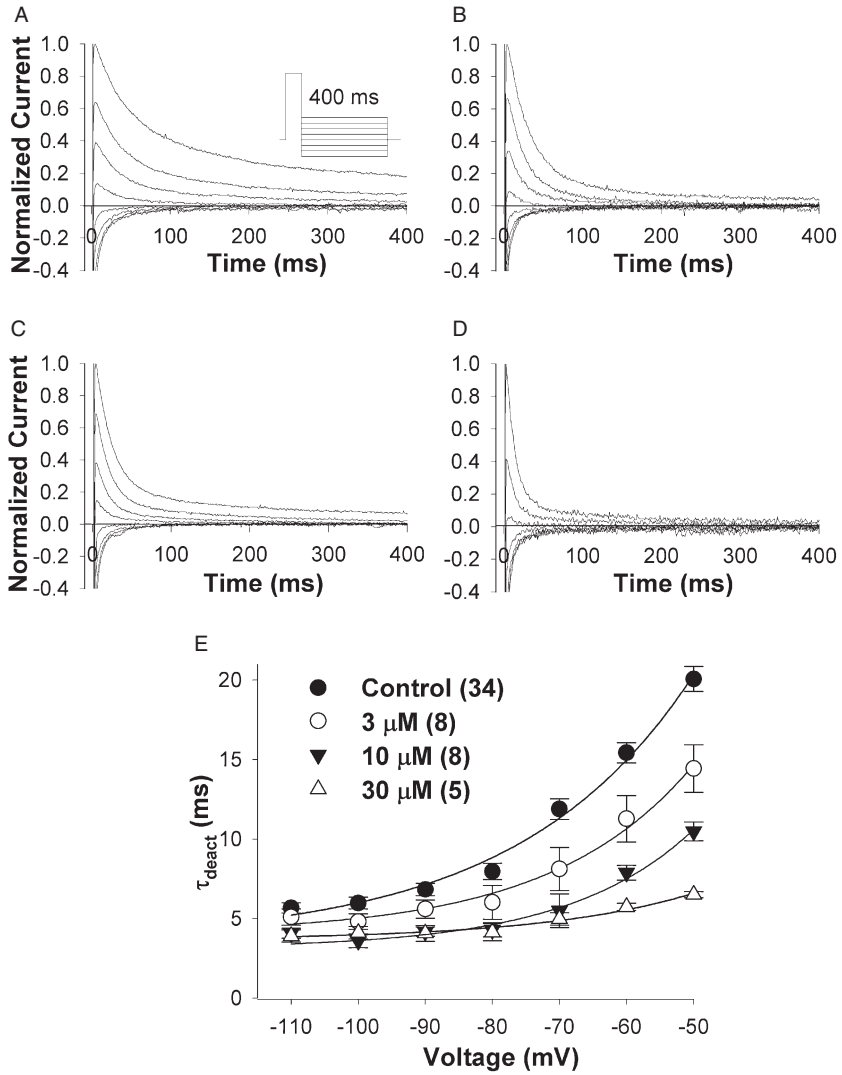

Figure 3 Effects of celecoxib on deactivation of $rK_v2.1$ channels. Normalized experimental current traces under control conditions (A) and in the presence of 3 μM (B), 10 μM (C), and 30 μM (D) celecoxib are shown. A two-pulse protocol was used: a P1 from a HP of –80 mV to +40 mV was followed by a P2 ranging between –40 and –110 mV in –10 mV increments (inset in panel A). (E) Voltage dependence of τ_{deact} in control conditions and in the presence of 3, 10, and 30 μM celecoxib. The values of τ_{deact} were obtained by fitting the time course of tail currents with a mono-exponential function; (*n*), number of experiments.

The fast and the slow time constants were, respectively, 0.54 ± 0.05 and 5.41 ± 0.38 s in control, 0.52 ± 0.05 and 3.76 ± 0.27 s ($P < 0.01$) at 3 μM, 0.60 ± 0.08 s and 3.35 ± 0.24 s ($P < 0.001$) at 10 μM, and 1.12 ± 0.06 s ($P < 0.001$) and 5.48 ± 0.32 s ($P < 0.01$, in comparison with 3 and 10 μM) at 30 μM (Figure 6, B and C). In addition, the fractional contribution of the fast component increased from 35.0 ± 3.8% in control to 55.0 ± 3.6% at 30 μM celecoxib (P < 0.01) (Figure 6D). Celecoxib, therefore, selectively accelerated the slow component of recovery at 3 and 10 μM and slowed both components of recovery at 30 μM.

Simulations

We next examined if the observed effects of celecoxib on the current could be explained solely by gating modifications described above. If so, then simulations based on kinetic parameters derived from experimental data would approximate experimental currents. For simulations, we used averaged experimental parameters of the kinetics of activation and inactivation in control and in the presence of 0.3, 1, 3, 10 and 30 μM celecoxib (see the section Computer Simulations in Methods). The traces were generated in Clampfit 9.0 (Figure 7). A comparison of the simulated and the experimental currents showed that the gating modification alone could not account for the decrease in peak currents, especially at higher concentrations of celecoxib (Figure 7E, F). For example, at +40 mV, the simulated peak current amplitude at 10 μM was 0.83 ± 0.03 of the control value, while the experimental current reached only 0.55 ± 0.10. This discrepancy in peak amplitudes was more prominent at 30 μM (+40 mV): 0.63 ± 0.03 versus 0.15 ± 0.05 for simulation and experiment, respectively. A small difference between experimental and simulated currents was observed at 1 and 3 μM celecoxib as well.

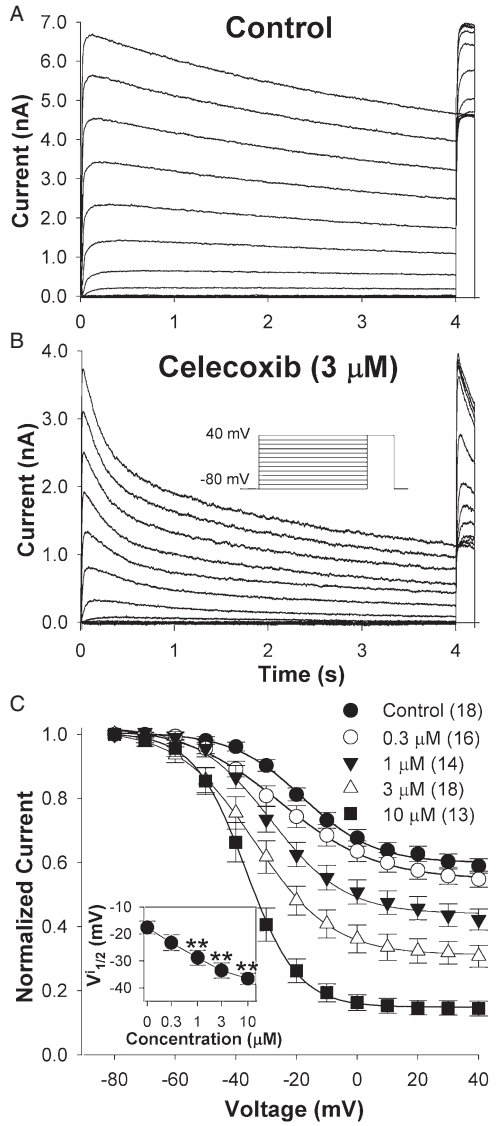

Figure 4 Effects of celecoxib on steady-state inactivation of $rK_v2.1$ channels. Steady-state inactivation was determined by using a two-pulse protocol: a 4000 ms pulse from a HP of –80 mV to potentials between –80 and +40 mV in 10 mV increments (P1) was followed by a 250 ms pulse to +40 mV (P2) (inset in panel B). Experimental current traces are shown under control conditions (A) and at 3 μM celecoxib (B). Celecoxib accelerated inactivation of the $rK_v2.1$ current (C) and caused a hyperpolarizing shift of the half-inactivation potential (inset) in concentration-dependent manner. The $V^i_{1/2}$ values were determined by fitting steady-state inactivation relations with a Boltzmann function $f_i(V) = 1/(1 + \exp(-(V^i_{1/2} - V)/k)) + C_{i0}$, where k is the slope factor, C_{i0} is the constant, and (*n*) is the number of experiments.

We analysed the fraction of block that was defined as the difference between the peak currents in simulation and those in experimental recordings. This fraction of block was voltage dependent, with a greater block at more negative test potentials (Figure 8). For example, in the presence of 10 μM celecoxib, the differences between normalized simulated and experimental currents were 0.58 ± 0.12 at –30 mV and 0.28 ± 0.14 at +40 mV, respectively (Figure 8).

Closed-channel block

The discrepancy between the simulated and the experimental currents implied additional inhibitory effects of celecoxib. We therefore assessed if celecoxib could block the channels in the closed state, by using a 0.2 Hz train consisting of 40-ms pulses to +40 mV from a HP of –80 mV. If celecoxib blocked the channel in the closed state at –80 mV, then the amplitude of the current during short 40-ms depolarization pulses to +40 mV would indicate the fraction of non-blocked channels, albeit with the gating characteristics modified by celecoxib. A typical time course of the peak current upon application and subsequent washout of 10 μM celecoxib is shown in Figure 9A. During the first three or four pulses after the beginning of celecoxib application, we observed a monotonic decrease in the current amplitude (Figure 9A). This decrease in current, from the end of one pulse to the peak of the following pulse, occurred during the interpulse interval, with the cell clamped at –80 mV, clearly indicating drug effect on the closed channel. The application of 10 μM celecoxib reduced the current, with a time constant of 22 ± 3 s (n = 16). The inhibition was completely reversible, with a recovery time constant of 27 ± 5 s (n = 12).

A closed-channel block can slow down activation of the whole-cell current (Bouchard and Fedida, 1995; Milnes *et al.*, 2003). Therefore, we determined the time constants of activation before and during application of 10 μM celecoxib, as previously described (see Methods and Figure 2). The time course of τ_{act} normalized to the control value and the corresponding peak current amplitude are shown in Figure 9B. The value of normalized τ_{act} first rapidly decreased to a minimum of 0.77 ± 0.03 and then slowly increased until it reached a steady-state level of 0.93 ± 0.04 (about 150 s after the beginning of drug application). The latter value was close to the ratio of averaged τ_{act} at 10 μM to that of the control (0.94 ± 0.15) determined during continuous exposure of HEK-293 cells to the drug (Figure 2C). The slow increase of τ_{act} was accompanied by consistent reduction in peak current (Figure 9B). The difference between the τ_{act} at minimum and at the end of drug application session was statistically significant ($P < 0.05$, paired *t*-test).

To further substantiate the role of closed channel block, we examined the time course of peak current after exposure of cells held at –80 mV to 30 μM celecoxib without electric stimulation. The protocol consisted of ten 100-ms pulses every 5 s to +40 mV under control conditions, a rapid application of 30 μM celecoxib to the bath with the cells held at –80 mV without stimulation and resumption of 0.2 Hz stimulation after 5-min-long exposure (Figure 9C,D). The cells were exposed to the drug under stimulus-free conditions for 5 min so as to ensure that the closed-channel block had developed completely by the time the stimulus was resumed. The amplitude of the first pulse in the presence of drug, after this stimulus-free exposure for 5 min, was 58 ± 6 % of control, suggesting an effect of celecoxib on the closed channels at ~80 mV. Current amplitude was further reduced by ~15% during the next five pulses and then slowly decreased until stabilizing at 18% of control after 15 min in the presence of the drug (Figure 9D). The latter

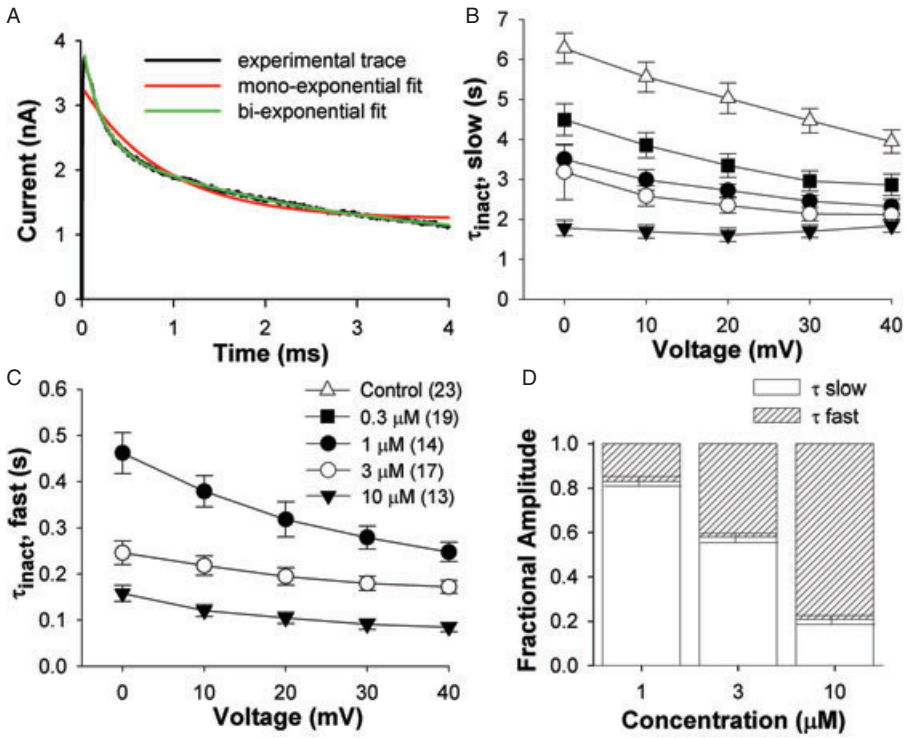

Figure 5 Effects of celecoxib on kinetics of open-state inactivation of $rK_v2.1$ channels. Inactivation kinetics were determined by using 4000 ms pulses between 0 and +40 mV (HP = –80 mV) in control and at different concentrations of celecoxib. Decay phases of the current traces were fitted with a single exponential function in control conditions and at 0.3 μM celecoxib, and with a bi-exponential function at 1, 3, and 10 μM celecoxib. (A) Fitting results of representative inactivation current trace (+40 mV, 3 μM celecoxib) with bi-exponential (time constants of 0.20 and 2.58 s) and mono-exponential (time constant of 1.01 s) functions. (B) Voltage dependence of τ_{inact} in control conditions and with 0.3 μM celecoxib, along with the slow component of inactivation at 1, 3, and 10 μM celecoxib. (C) Voltage dependence of the fast component of inactivation at 1, 3, and 10 μM celecoxib. (D) Fractional contributions of the slow and the fast components of open-state inactivation at 1, 3, and 10 μM celecoxib.

value is consistent with the current amplitude in the cells constantly exposed to 30 μM celecoxib (16.4% of control value).

Open-channel block

After keeping the cell at –80 mV in 30 μM celecoxib for 5 min without stimulation, the current showed a rapid decline for the first few pulses, indicative of a use-dependent inhibition, which is a feature of open-channel block (Qu *et al.*, 2007). To examine if an open-channel block could contribute to the peak current reduction, we tested the use dependence of inhibition at 10 and 30 μM celecoxib (Figure 10). As the current peaked at 30 ms and the fast time constant of inactivation was 85 ms (at +40 mV, 10 μM celecoxib), we could expect that inactivation would reduce the peak current substantially during a 40-ms pulse. Therefore, that for the acceleration of inactivation caused by gating modification would not mask use dependence of the open-channel block to be ensured, stimulation frequency of 0.2 Hz was selected. A 5-s interpulse interval was selected because the recovery from inactivation was nearly complete within 5 s and the interpulse interval was less than the time constant of recovery from inhibition (27 s). The value of normalized current in Figure 10 represents a ratio of the maximum current in the presence of the drug to that in the absence of the drug in the same cycle. The data showed use-dependent inhibition at 30 μM but not at 10 μM, suggesting open-channel block at higher concentrations of celecoxib (Figure 10).

Discussion and conclusions

Celecoxib, a selective COX-2 inhibitor and a widely prescribed NSAID, has now been shown to inhibit ion channels and affect cellular physiology independently of COX inhibition (Park *et al.*, 2007; Zhang *et al.*, 2007; Frolov *et al.*, 2008a,b). Because of the significance of selective COX-2 inhibitors in treating many conditions in general and because of the prevalent use of celecoxib (Celebrex) in particular, it is important to understand the mechanisms underlying its action on ion channels. The data presented here provide information on how celecoxib reduces current amplitude and dramatically accelerates kinetics of $rK_v2.1$ channels in dose-dependent manner.

As $K_v2.1$ channels are expressed in neural and cardiac tissues of several species, they are subject of intensive studies for recent years (Klemic *et al.*, 1998; Kerschensteiner *et al.*, 2003; Vega-Saenz de Miera, 2004; Zhang *et al.*, 2004; Tammaro *et al.*, 2005; Mohapatra and Trimmer, 2006). The kinetic data in this study in general are consistent with those

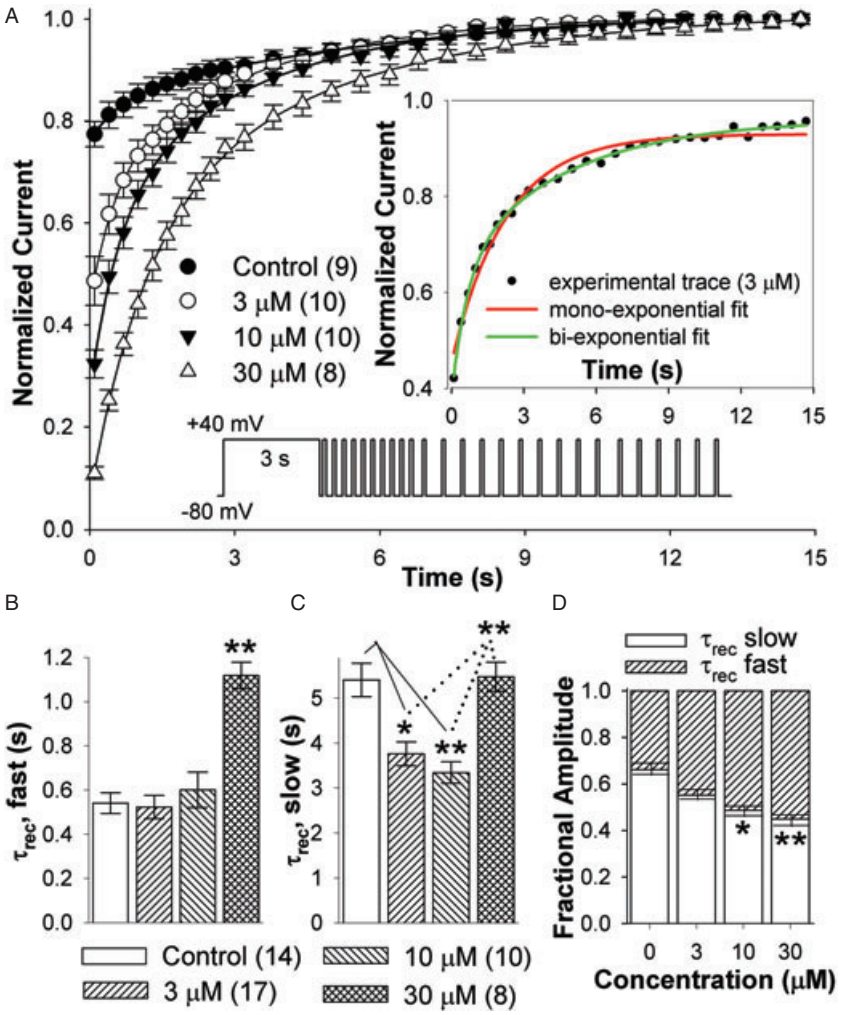

Figure 6 Effects of celecoxib on the recovery of $rK_v2.1$ channels from inactivation. (A) Normalized peak currents are plotted as function of interpulse interval in control and during exposure to 3, 10 or 30 μM celecoxib. A standard two-pulse protocol was used: a 3000 ms P1 to +40 mV (HP = –80 mV) was followed by a 100-ms P2 to +40 mV, with the interval between P1 and P2 varying from 100 to 17800 ms. For a better resolution of the initial phase of recovery, the time intervals between consecutive P2 test pulses were shorter during the first 3 s of recovery. Recovery kinetics were best described by a bi-exponential function. *Inset*, fitting results of a representative recovery current trace (–80 mV, 3 μM celecoxib) with bi-exponential (time constants of 0.66 and 4.58 s) and mono-exponential (time constant of 2.25 s) functions. Bar plots summarize the effects of celecoxib on the fast (B) and the slow (C) components of recovery, and their fractional amplitudes (D); (*n*), number of experiments.

in previously published results on $K_v2.1$ channels (Table 1). For example, values of half-activation potential $V^a_{1/2}$ obtained by using single power Boltzmann equation vary between –11.8 ± 2.7 mV and 16.4 ± 0.6 mV (VanDongen *et al.*, 1990; Kurata *et al.*, 2002; Kerschensteiner *et al.*, 2003; Madeja *et al.*, 2003; Tammaro *et al.*, 2005; Mohapatra and Trimmer, 2006) when $K_v2.1$ channels were studied in different expression systems. Our value of $V^a_{1/2}$ –1.7 ± 1.1 mV in control, if fitted with the single power Boltzmann function, is in the same range of voltage. Kinetics of $K_v2.1$ channel activation in our study is also consistent with the results from other groups. For example, our data for τ_{act} at +40 mV determined by fitting a rising phase of the current with a mono-exponential function elicited 14.2 ± 0.5 ms. This value is close to the corresponding activation time constants ~14 ms and ~17 ms obtained by Madeja *et al*. (Madeja *et al.*, 2003) and Vega-Saenz de Miera (2004), respectively. Our $K_v2.1$ deactivation time constants of 5.7 ± 0.3 at –110 mV and 20 ± 1 ms at –50 mV are also close to those obtained by Madeja *et al*. (2003), 4 ± 1 ms at –120 mV and 17 ± 1 ms at –40 mV.

There are some similarities and some differences in published studies of inactivation properties of $K_v2.1$ channels. Voltage dependence of steady-state inactivation relationships for $K_v2.1$ channels shows a clear U-shape in some studies (Klemic *et al.*, 1998; Kurata *et al.*, 2002; Kerschensteiner *et al.*, 2003), while a U-shape is less apparent or absent in data from others (Zhang *et al.*, 2004; Tammaro *et al.*, 2005; Mohapatra and Trimmer, 2006). Our data on the inactivation of $K_v2.1$ channels fall in the latter category. The presence or absence of a U-shape in inactivation curves depends on several factors such as the expression system used, solutions and voltage-clamp protocols employed (Klemic *et al.*, 1998; Kurata *et al.*, 2002; Kerschensteiner *et al.*, 2003; Vega-Saenz de Miera, 2004; Zhang *et al.*, 2004, Tammaro *et al.*, 2005; Mohapatra and

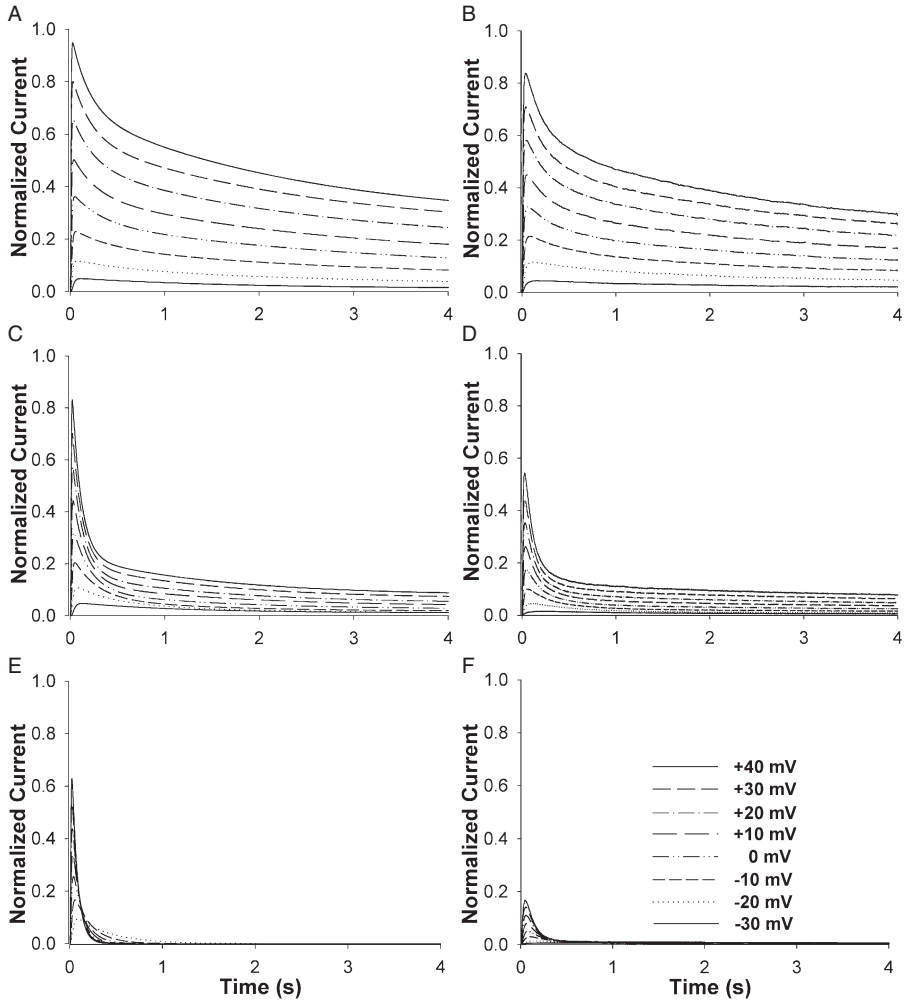

Figure 7 Comparison of the simulated and the experimental currents at different concentrations of celecoxib. To evaluate if gating modifications could exclusively account for the inhibition of $rK_v2.1$ channel current, simulated currents were generated with Clampfit 9.0 by using averaged experimental parameters of activation and inactivation in control and at different concentrations of celecoxib. The simulated (A, C, E) and the averaged experimental (B, D, F) current traces are shown for 4000 ms voltage steps between −30 and +40 mV from a HP of −80 mV at 3, 10, and 30 μM celecoxib. The currents in the presence of different concentrations of celecoxib were normalized to the peak current under control conditions (data not shown).

Trimmer, 2006). Kinetics of inactivation demonstrate an increase in inactivation time constant with voltage (Vega-Saenz de Miera, 2004) or show both decreasing and increasing part of the voltage dependence (VanDongen *et al.*, 1990; Kerschensteiner *et al.*, 2003). Our data on inactivation of $K_v2.1$ channels, under control conditions, showed decreasing voltage dependence of the inactivation time constant, with the value 4.2 ± 1.1 s (+40 mV) that is within the range obtained by others, from 3.3 to 6 s (VanDongen *et al.*, 1990; Kerschensteiner *et al.*, 2003; Madeja *et al.*, 2003; Vega-Saenz de Miera, 2004; Tammaro *et al.*, 2005; Mohapatra and Trimmer, 2006). Recovery from inactivation, determined by using a mono-exponential function has been reported to be approximately 2.2 s at −80 mV when $K_v2.1$ channels are expressed in oocytes (Kerschensteiner *et al.*, 2003), with our study showing a value of 3.6 ± 0.2 s.

Our data indicate that acceleration of inactivation was the paramount aspect of celecoxib effects, which significantly contributed to the reduction in the current at relatively low concentrations (≤10 μM). The $rK_v2.1$ channel is known to inactivate very slowly; it is believed that the channel lacks N-type inactivation (Gebauer *et al.*, 2004). Our data also showed only a slow component of inactivation under control conditions. However, exposure of the channel to celecoxib unmasked a fast component of inactivation, with a time constant that was an order of magnitude faster than that of the slow component.

The time course of recovery of $K_v2.1$ channels from inactivation has been reported to be mono-exponential (Klemic *et al.*, 1998; Kerschensteiner and Stocker, 1999). However, our data revealed the presence of two components of recovery in control as well as in the presence of the drug. This was possibly due to a better resolution of the initial phase of recovery using shorter time intervals between pulses during the first 3 s of recovery. The presence of two components of recovery usually indicates availability of two distinct inactivation mechanisms in the channel (Figures 5C and 6D). Thus, in addition to examining the

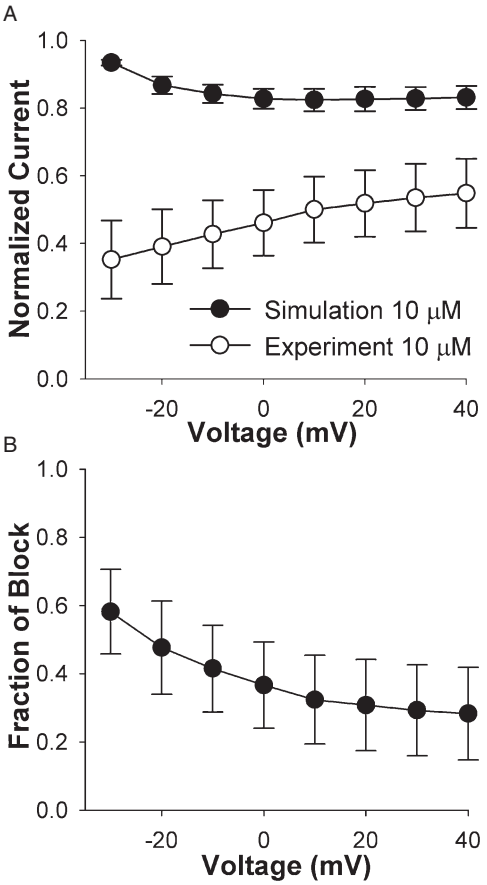

Figure 8 Block of $rK_v2.1$ channels by celecoxib. (A) Voltage dependence of the peak current inhibition in the presence of 10 μM celecoxib is shown for the averaged simulated and experimental currents. (B) Voltage dependence of the current reduction that is in excess of the inhibition due to change in kinetics; data were obtained by subtracting experimental from the simulated values shown in panel A.

effect of celecoxib on channel kinetics, we were able to observe two components of inactivation in the presence of this compound and two components of recovery from inactivation, both in the presence and the absence of celecoxib.

Our data do not support the hypothesis of open-channel block at low concentrations (≤10 μM). First, there is a clear acceleration of deactivation upon the application of celecoxib (Figure 3). In contrast, an open-channel block is characterized by slower deactivation kinetics than in control and by a 'cross-over' of tail currents (Gonzalez *et al.*, 2002; Wang *et al.*, 2003). In principle, the concentration-dependent acceleration of deactivation (Figure 3) could conceivably obscure any effects on deactivation arising from a putative open-channel block at higher concentrations. To further assess the possibility of open-channel block, we examined the effects of the drug on recovery from inactivation. While dissociation of an open-channel blocker at repolarizing membrane potentials can slow down recovery from inactivation (Bouchard and Fedida, 1995; Wang *et al.*, 2003; Qu *et al.*, 2007), recovery was accelerated in the presence of 3 and 10 μM celecoxib (Figure 6), suggesting modification of channel gating at these concentrations. These factors, along with the absence of use dependence at 10 μM, argue against the possibility of an open-channel block at ≤10 μM celecoxib or the possibility that the significant closed-channel block observed at low concentrations might arise from a low but finite probability of opening, allowing the drug to enter the channel pore and block it. In contrast, the application of 30 μM celecoxib caused a slowing of recovery and showed use dependence of action. These results support the view that, while celecoxib did not induce open-channel block at concentrations ≤10 μM, at higher concentrations, this compound blocked a substantial fraction of $rK_v2.1$ channels in the open state. In the context of open-channel block at high concentrations, our data on deactivation indicate that two opposite mechanisms, acceleration due to gating modification and deceleration because of open-channel block, could contribute to the observed behaviour of τ_{deact}. As the strength of these effects can be different, acceleration of deactivation may partially compensate for the slowing of deactivation due to open-channel block at higher concentrations.

The data presented here suggest several different reversible effects of celecoxib on $rK_v2.1$ channels. At relatively low concentrations (≤3 μM), celecoxib accelerated activation, deactivation, inactivation and the slow component of recovery from inactivation. At higher concentrations (≤10 μM), celecoxib also caused a slowly developing closed-channel block that was accompanied by relative slowing of activation, and open-channel block that was evident at 30 μM celecoxib. Similar observations have been reported for block of $K_v1.5$ channels by 4-aminopyridine (4-AP) (Bouchard and Fedida, 1995). At lower concentrations, 4-AP modified gating of $K_v1.5$ current, whereas, at higher doses, it exerted closed- and open-channel blocks (Bouchard and Fedida, 1995). The rapid onset and recovery from inhibition seen in our experiments are not consistent with channel internalization and/or trafficking as a factor of current reduction. O'Connell and Tamkun (2005) have shown that the characteristic time constant of $K_v2.1$ channels trafficking to plasma membrane in HEK-293 cells is about 20 min, which is considerably longer than the time constant of recovery from inhibition by celecoxib (Figure 9A).

Our data show that celecoxib significantly inhibited $K_v2.1$ channels over the range of therapeutic concentrations, from 1.7 to 6.2 μM (Davies *et al.*, 2000). The concentration is higher in certain conditions, for example, in the case of moderate hepatic impairment or coadministration of certain drugs, such as ketaconazole (Davies *et al.*, 2000). It is worth noting that a significant effect on cellular physiology is often mediated by a much smaller effect at the molecular level. For example, while celecoxib inhibits Na^+ channels in third-order rat retinal neurones with an IC_{50} of 5.2 μM, a relatively mild inhibition of the channels can lead to a significant reduction in spontaneous firing frequency of these neurones, with an IC_{50} of 0.76 μM (Frolov *et al.*, 2008a). $K_v2.1$ channels are expressed in several tissues including heart, pancreas, pulmonary arteries, placental vasculature, and hippocampal and cortical pyramidal neurones (Misonou *et al.*, 2004; Ordog *et al.*, 2006; Park *et al.*, 2006). A reduction in $K_v2.1$ current due to hyperpolarizing shift of half-inactivation potential, acceleration of inactivation, and channel block by celecoxib is likely to affect repolarization, prolong action potentials and

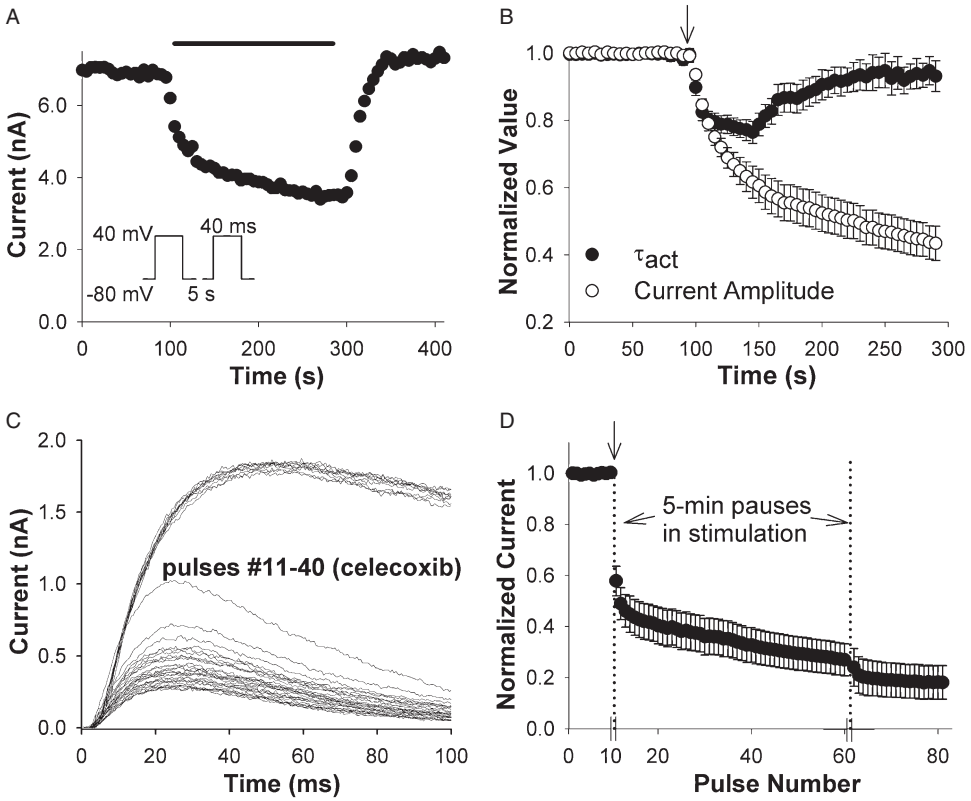

Figure 9 Development of $rK_v2.1$ inhibition by celecoxib. (A) Time course of peak current inhibition during exposure to 10 μM celecoxib (horizontal bar). Currents were elicited by 0.2 Hz pulse trains consisting of 40-ms pulses to +40 mV (HP = –80 mV) (shown in inset). Time constant for the onset of inhibition was 22 ± 3 s (n = 16), and time constant for the recovery from inhibition during wash-out was 27 ± 5 s (n = 12). (B) after application of 10 μM celecoxib (arrow), the activation time constants τ_{act} initially rapidly decreased (gating modification) and then slowly increased following the development of closed-channel block (reduction of peak currents, open circles) (n = 13). (C, D), development of peak current inhibition after 5-min exposure to 30 μM celecoxib in the absence of stimulation (cells held at –80 mV). Currents were elicited by 100-ms pulses to +40 mV (0.2 Hz, HP = –80 mV). Representative current traces (C) are shown in control (pulses # 1–10) and after 5-min exposure to 30 μM celecoxib (pulses #11–40). (D) Averaged normalized time course for the development of inhibition (n = 8). Steady-state inhibition is observed 15 min after application of the drug (vertical arrow). The cells were exposed to celecoxib by using a custom-made perfusion system.

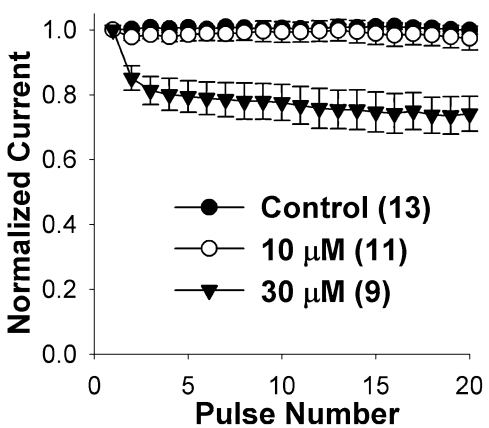

Figure 10 Use dependence of $rK_v2.1$ channel inhibition by celecoxib. The currents were elicited by 0.2 Hz pulse trains consisting of 40 ms pulses to +40 mV from a HP of –80 mV in control and during the continuous presence of 10 or 30 μM celecoxib in the bath. Peak currents were normalized to the peak current amplitude obtained during the first pulse in the train; (n), number of experiments. The data showed use-dependent inhibition at 30 μM but not at 10 μM celecoxib.

affect the functioning of the tissues in which the channels play a significant physiological role. In cardiac cells, action potential prolongation is one of the major causes for prodysrhythmic events, such as early afterdepolarizations and dysrhythmias, such as torsade de pointes (Wit and Rosen, 1992). For example, $K_v2.1$ channels form the molecular basis of a major repolarizing current, $I_{K,slow2}$, in mice (Xu *et al.*, 1999). Reduction of the current carried by $K_v2.1$ channels due to their rapid inactivation or channel block can induce cardiac arrhythmia. Indeed, transgenic mice expressing a dominant-negative $K_v2.1$ α-subunit demonstrate both prolongation of action potential duration and spontaneous triggered activity (Xu *et al.*, 1999). Similarly, inhibition of K_v2 channels by celecoxib underlies the induction of dysrhythmia in *Drosophila* heart and in rat heart cells in culture (Frolov *et al.*, 2008b). The observations shown here provide a possible mechanism for such effect. Celecoxib has also been shown to inhibit Na^+ channels in rat dorsal root ganglion neurones (Park *et al.*, 2007) and Ca^{2+} channels in rat pheochromocytoma (PC12) cells (Zhang *et al.*, 2007). Therefore, this compound is likely to have adverse effects on the functioning of other tissues. In line with this argument, experiments on rat retinas suggest an effect of the drug on second- and

Table 1 Comparison of some gating parameters of $K_v2.1$ channels under control conditions, obtained in this study and in the studies of other research groups

Parameter	*Our value*	*Values from other groups*	*Reference*
Half-activation potential ($V^a_{1/2}$)	–31.8 ± 1.3 mV	–9.2 ± 3.8 mV*	VanDongen *et al.* (1990)
		–2.8 ± 1.7 mV*	Kurata *et al.* (2002)
	–1.7 ± 1.1 mV*	2.4 mV*	Madeja *et al.* (2003)
		3 ± 1 mV*	Kerschensteiner *et al.* (2003)
		–11.8 ± 2.7 mV*	Tammaro *et al.* (2005)
		16.4 ± 0.6 mV*	Mohapatra and Trimmer (2006)
Activation time constant τ_{act}	4.5 ± 0.3 s (+40 mV)	~14 ms (+40 mV)**	Madeja *et al.* (2003)
	14.2 ± 0.5 ms (+40 mV)**	~17 ms (+40 mV)**	Vega-Saenz de Miera (2004)
Deactivation time constant τ_{deact}	20 ± 1 ms (–50 mV)	~6 and ~2 ms (–50 mV)	VanDongen *et al.* (1990)
		17 ± 1 ms (–40 mV)	Madeja *et al.* (2003)
	5.7 ± 0.3 ms (–110 mV)	4 ± 1 ms (–120 mV)	Madeja *et al.* (2003)
Half-inactivation potential ($V^i_{1/2}$)	–17.6 ± 2.3 mV (4 s pulse)	–19.0 ± 1.5 mV (10 s pulse)	VanDongen *et al.* (1990)
		–26.3 ± 0.7 mV (5 s pulse)	Kurata *et al.* (2002)
		–26.2 ± 0.4 mV (10 s pulse)	Mohapatra and Trimmer (2006)
Inactivation time constant τ_{inact}	3.9 ± 0.3 s (+40 mV)	~4.5 s (+20 mV)	VanDongen *et al.* (1990)
		6 s (+40 mV)	Kerschensteiner *et al.* (2003)
		~3.3 s (+40 mV)	Vega-Saenz de Miera (2004)
Recovery from inactivation time constant τ_{rec}	0.54 ± 0.05 s (fast)	1.5 s (–90 mV)**	Klemic *et al.* (1998)
		2.2 s (–80 mV)**	Kerschensteiner *et al.* (2003)
	5.4 ± 0.3 s (slow)		
	3.6 ± 0.2 s**		

*Obtained by using single power Boltzmann equation.
**Time course fitted with a mono-exponential function.

third-order retinal neurones (Frolov *et al.*, 2008a). Thus, the data presented in our paper on the mode of action of celecoxib on $rK_v2.1$ channels will be helpful in further analysing the effects of this drug on ion channels in general, as well as in understanding the adverse effects of celecoxib in various tissues.

Acknowledgements

We are thankful to Dr. Michael R. Detty, Mr. Bryan R. Wetzel and Mr. Michael K. Gannon for the purification and characterization of celecoxib. We are thankful to Dr. M. Slaughter for providing the experimental setup and to Mrs. Irina Ignatova and Mr. Jason Myers for helping with experiments. This work was supported by Grants MCB-0094477 and MCB-0322461 from the National Science Foundation.

Conflicts of interest

The authors state no conflict of interest.

References

Alexander SP, Mathie A, Peters JA (2008). Guide to receptors and channels (GRAC), 3rd edition. *Br J Pharmacol* **153** (Suppl. 2): S1–209.

Baranauskas G, Tkatch T, Surmeier DJ (1999). Delayed rectifier currents in rat globus pallidus neurons are attributable to $K_v2.1$ and $K_v3.1/3.2$ K(+) channels. *J Neurosci* **19**: 6394–6404.

Birnbaum SG, Varga AW, Yuan LL, Anderson AE, Sweatt JD, Schrader LA (2004). Structure and function of K_v4-family transient potassium channels. *Physiol Rev* **84**: 803–833.

Bouchard R, Fedida D (1995). Closed- and open-state binding of 4-aminopyridine to the cloned human potassium channel $K_v1.5$. *J Pharmacol Exp Ther* **275**: 864–876.

Brownstein JS, Sordo M, Kohane IS, Mandl KD (2007). The tell-tale heart: Population-based surveillance reveals an association of rofecoxib and celecoxib with myocardial infarction. *PLoS ONE* **2**: e840.

Burnier M (2005). The safety of rofecoxib. *Expert Opin Drug Saf* **4**: 491–499.

Chopra M, Gu GG, Singh S (2000). Mutations affecting the delayed rectifier potassium current in Drosophila. *J Neurogenet* **14**: 107–123.

Davies NM, McLachlan AJ, Day RO, Williams KM (2000). Clinical pharmacokinetics and pharmacodynamics of celecoxib: a selective cyclo-oxygenase-2 inhibitor. *Clin Pharmacokinet* **38**: 225–242.

Flower RJ (2003). The development of COX2 inhibitors. *Nat Rev Drug Discov* **2**: 179–191.

Frolov RV, Slaughter MM, Singh S (2008a). Effects of celecoxib on ionic currents and spontaneous firing in rat retinal neurons. *Neuroscience* **154**: 1525–1532.

Frolov RV, Berim IG, Singh S (2008b). Inhibition of delayed rectifier potassium channels and induction of arrhythmia: a nosel effect of celecoxib and the mechanism underlying it. *J Biol Chem* **283**: 1518–1524.

Gebauer M, Isbrandt D, Sauter K, Callsen B, Nolting A, Pongs O *et al.* (2004). N-type inactivation features of $K_v4.2$ channel gating. *Biophys J* **86**: 210–223.

Gonzalez T, Navarro-Polanco R, Arias C, Caballero R, Moreno I, Delpon E *et al.* (2002). Assembly with the Kvbeta1.3 subunit modulates drug block of $hK_v1.5$ channels. *Mol Pharmacol* **62**: 1456–1463.

Hegde P, Gu GG, Chen D, Free SJ, Singh S (1999). Mutational analysis of the Shab-encoded delayed rectifier K(+) channels in Drosophila. *J Biol Chem* **274**: 22109–22113.

Kalgutkar AS, Crews BC, Rowlinson SW, Garner C, Seibert K, Marnett LJ (1998). Aspirin-like molecules that covalently inactivate cyclooxygenase-2. *Science* **280**: 1268–1270.

Kerschensteiner D, Stocker M (1999). Heteromeric assembly of $K_v2.1$ with $K_v9.3$: effect on the state dependence of inactivation. *Biophys J* **77**: 248–257.

Kerschensteiner D, Monje F, Stocker M (2003). Structural determinants of the regulation of the voltage-gated potassium channel

$K_v2.1$ by the modulatory alpha-subunit $K_v9.3$. *J Biol Chem* **278**: 18154–18161.

Klemic KG, Shieh CC, Kirsch GE, Jones SW (1998). Inactivation of $K_v2.1$ potassium channels. *Biophys J* **74**: 1779–1789.

Kurata HT, Soon GS, Eldstrom JR, Lu GW, Steele DF, Fedida D (2002). Amino-terminal determinants of U-type inactivation of voltage-gated K+ channels. *J Biol Chem* **277**: 29045–29053.

Leung YM, Kang Y, Gao X, Xia F, Xie H, Sheu L *et al*. (2003). Syntaxin 1A binds to the cytoplasmic C terminus of $K_v2.1$ to regulate channel gating and trafficking. *J Biol Chem* **278**: 17532–17538.

Madeja M, Leicher T, Friederich P, Punke MA, Haverkamp W, Musshoff U *et al*. (2003). Molecular site of action of the antiarrhythmic drug propafenone at the voltage-operated potassium channel $K_v2.1$. *Mol Pharmacol* **63**: 547–556.

Malin SA, Nerbonne JM (2002). Delayed rectifier K+ currents, IK, are encoded by K_v2 alpha-subunits and regulate tonic firing in mammalian sympathetic neurons. *J Neurosci* **22**: 10094–10105.

Milnes JT, Dempsey CE, Ridley JM, Crociani O, Arcangeli A, Hancox JC *et al*. (2003). Preferential closed channel blockade of HERG potassium currents by chemically synthesised BeKm-1 scorpion toxin. *FEBS Lett* **547**: 20–26.

Misonou H, Mohapatra DP, Park EW, Leung V, Zhen D, Misonou K *et al*. (2004). Regulation of ion channel localization and phosphorylation by neuronal activity. *Nat Neurosci* **7**: 711–718.

Misonou H, Mohapatra DP, Trimmer JS (2005). $K_v2.1$: a voltage-gated k+ channel critical to dynamic control of neuronal excitability. *Neurotoxicology* **26**: 743–752.

Mohapatra DP, Trimmer JS (2006). The $K_v2.1$ C terminus can autonomously transfer $K_v2.1$-like phosphorylation-dependent localization, voltage-dependent gating, and muscarinic modulation to diverse K_v channels. *J Neurosci* **26**: 685–695.

Mohapatra DP, Park KS, Trimmer JS (2007). Dynamic regulation of the $_v$oltage-gated $K_v2.1$ potassium channel by multisite phosphorylation. *Biochem Soc Trans* **35**: 1064–1068.

Murakoshi H, Trimmer JS (1999). Identification of the $K_v2.1$ K+ channel as a major component of the delayed rectifier K+ current in rat hippocampal neurons. *J Neurosci* **19**: 1728–1735.

O'Connell KM, Tamkun MM (2005). Targeting of voltage-gated potassium channel isoforms to distinct cell surface microdomains. *J Cell Sci* **118**: 2155–2166.

Ordog B, Brutyo E, Puskas LG, Papp JG, Varro A, Szabad J *et al*. (2006). Gene expression profiling of human cardiac potassium and sodium channels. *Int J Cardiol* **111**: 386–393.

Park KS, Mohapatra DP, Misonou H, Trimmer JS (2006). Graded regulation of the $K_v2.1$ potassium channel by variable phosphorylation. *Science* **313**: 976–979.

Park SY, Kim TH, Kim HI, Shin YK, Lee CS, Park M *et al*. (2007). Celecoxib inhibits Na+ currents in rat dorsal root ganglion neurons. *Brain Res* **1148**: 53–61.

Patel AJ, Lazdunski M, Honore E (1997). $K_v2.1/K_v9.3$, a novel ATP-dependent delayed-rectifier K+ channel in oxygen-sensitive pulmonary artery myocytes. *EMBO J* **16**: 6615–6625.

Pinto LH, Klumpp DJ (1998). Localization of potassium channels in the retina. *Prog Retin Eye Res* **17**: 207–230.

Qu YJ, Bondarenko VE, Xie C, Wang S, Awayda MS, Strauss HC *et al*. (2007). W-7 modulates $K_v4.3$: pore block and Ca2+-calmodulin inhibition. *Am J Physiol Heart Circ Physiol* **292**: H2364–2377.

Singh A, Singh S (1999). Unmasking of a novel potassium current in Drosophila by a mutation and drugs. *J Neurosci* **19**: 6838–6843.

Singh G, Triadafilopoulos G (1999). Epidemiology of NSAID induced gastrointestinal complications. *J Rheumatol* Suppl **56**: 18–24.

Tammaro P, Smirnov SV, Moran O (2005). Effects of intracellular magnesium on $K_v1.5$ and $K_v2.1$ potassium channels. *Eur Biophys J* **34**: 42–51.

VanDongen AM, Frech GC, Drewe JA, Joho RH, Brown AM (1990). Alteration and restoration of K+ channel function by deletions at the N- and C-termini. *Neuron* **5**: 433–443.

Vega-Saenz de Miera EC (2004). Modification of $K_v2.1$ K+ currents by the silent K_v10 subunits. *Brain Res Mol Brain Res* **123**: 91–103.

Wang S, Morales MJ, Qu YJ, Bett GC, Strauss HC, Rasmusson RL (2003). $K_v1.4$ channel block by quinidine: evidence for a drug-induced allosteric effect. *J Physiol* **546**: 387–401.

Wang S, Bondarenko VE, Qu Y, Morales MJ, Rasmusson RL, Strauss HC (2004). Activation properties of $K_v4.3$ channels: time, voltage and [K+]o dependence. *J Physiol* **557**: 705–717.

Wang W, Hino N, Yamasaki H, Aoki T, Ochi R (2002). $K_v2.1$ K+ channels underlie major voltage-gated K+ outward current in H9c2 myoblasts. *Jpn J Physiol* **52**: 507–514.

Wareing M, Bai X, Seghier F, Turner CM, Greenwood SL, Baker PN *et al*. (2006). Expression and function of potassium channels in the human placental vasculature. *Am J Physiol Regul Integr Comp Physiol* **291**: R437–R446.

Weber A, Casini A, Heine A, Kuhn D, Supuran CT, Scozzafava A *et al*. (2004). Unexpected nanomolar inhibition of carbonic anhydrase by COX-2-selective celecoxib: new pharmacological opportunities due to related binding site recognition. *J Med Chem* **47**: 550–557.

Wit AL, Rosen MR (1992). After depolarizations and triggered activity: distinction from automaticity as an arrhythmogenic mechanism. In: Fozzard HA, Haber E, Jennings RB, Katz AM, Morgan HE (eds). *The Heart and Cardiovascular System*. Raven Press: New York, pp. 2113–2164.

Xu H, Barry DM, Li H, Brunet S, Guo W, Nerbonne JM (1999). Attenuation of the slow component of delayed rectification, action potential prolongation, and triggered activity in mice expressing a dominant-negative K_v2 alpha subunit. *Circ Res* **85**: 623–633.

Yan L, Figueroa DJ, Austin CP, Liu Y, Bugianesi RM, Slaughter RS *et al*. (2004). Expression of voltage-gated potassium channels in human and rhesus pancreatic islets. *Diabetes* **53**: 597–607.

Zhang HX, Zhang W, Jin HW, Wang XL (2004). Galantamine blocks cloned $K_v2.1$, but not $K_v1.5$ potassium channels. *Brain Res Mol Brain Res* **131**: 136–140.

Zhang Y, Tao J, Huang H, Ding G, Cheng Y, Sun W (2007). Effects of celecoxib on voltage-gated calcium channel currents in rat pheochromocytoma (PC12) cells. *Pharmacol Res* **56**: 267–274.